Additive Manufacturing 21 (2018) 76–83

Contents lists available at ScienceDirect

Additive Manufacturing

journal homepage: www.elsevier.com/locate/addma

Full Length Article

Liquid bridge microstereolithography

Jeongwoo Lee, Yanfeng Lu, Sumanth Kashyap, Aslan Alarmdari, Md. Omar Faruk Emon, Jae-Won Choi*

Department of Mechanical Engineering, The University of Akron, 244 Sumner Street, Akron, OH, 44325-3903, United States

ARTICLE INFO

Keywords:
Microstereolithography
Stereolithography
Liquid bridge
Photopolymerization
Surface tension
Additive manufacturing

ABSTRACT

Microstereolithography (MSL) has been employed to create 3D microstructures for a wide range of applications. Despite the many advantages of using this process, there are still several drawbacks such as the need to use a large amount of a material compared to the volume of the microstructure to be built, oxygen inhibition, and difficulty in processing highly viscous photopolymers. To minimize the amount of material required, the use of a liquid bridge has been suggested as a modification to the existing microstereolithography process. A liquid bridge can be easily found in nature after a rainfall. Basically, a bridge can be formed between two solid bodies, where surface tension can sustain a liquid bridge against a gravitational force, which tends to destroy it. With this natural phenomenon, a photopolymer can be intentionally formed between two substrates: a transparent substrate with a low surface energy can be used as a top substrate, while another substrate with a higher surface energy can be used to hold the fabricated structure together. This process, called *liquid bridge microstereolithography* (LBMSL), is advantageous since it uses a relatively small amount of a material, removes oxygen inhibition due to the constraint of the material surface, and offers the possibility of utilizing a highly viscous material. In this study, a mathematical model was taken to simulate a liquid bridge with a certain volume and height. Adhesion tests were accomplished to ensure the fabricated layer detaches from the top substrate while the fabricated structure remains attached to the bottom structure. Photopolymers with different viscosities were employed in LBMSL, and the results were compared with those in the traditional MSL. Finally, various 3D microstructures were fabricated by LBMSL; these fabricated microstructures provide compelling evidence that LBMSL is advantageous over the existing process for MSL.

1. Introduction

Since the concept of additive manufacturing (AM), also known as 3D printing, was proved in the early 1980s, various 3D printing processes have been developed. Representative processes include vat photopolymerization, powder bed fusion, extrusion, material/binder jetting, and beam deposition. Among the vat photopolymerization processes, stereolithography (SL) has been regarded as a high-resolution technique. Microstereolithography (MSL), which evolved from SL to obtain resolutions of a few microns on the *xy* plane and a few tens of microns along the vertical direction, has gained attention due to its superior capability to create “real” 3D microstructures since it was first introduced by Ikuta and Hirowatari [1–3]. There are two major MSL types depending on the method of layer creation; (1) projection MSL using a mask with light exposure for the entire layer [2,3] and (2) scanning MSL using a focused beam for contouring and hatching [4,5]. Elaborate 3D structures can be simply fabricated by UV beam exposure on photoreactive liquid resins and a subsequent curing reaction of the resins into solid polymer layer by layer [6]. Therefore, MSL has been widely adopted in the areas of biomedicals [7–10], tissue engineering [11,12], and microelectromechanical systems (MEMS) [13,14]. Although MSL has a superior capability in microstructuring, there are some limitations, including the requirement of a relatively large amount of material compared to the volume of the microstructure, oxygen inhibition, and difficulty in using highly viscous photopolymers, among others.

MSL requires a vat containing a photopolymer (hereafter referred to as *vat-based MSL*) [15]. A build platform is generally mounted to a Z-stage and positioned in the vat. In the top-down approach [2,16], the platform is first moved downward and then upward to refresh a photopolymer with a layer of material of a predetermined thickness (in contrast to the SL process, where no recoater is typically used). During this process, the fabricated part must be completely and evenly covered by a photopolymer; therefore, a relatively large amount of a photopolymer, as compared to the size of a fabricated microstructure, is required. While the bottom-up approach [17] and the material pumping

* Corresponding author.
E-mail address: jchoi1@uakron.edu (J.-W. Choi).

https://doi.org/10.1016/j.addma.2018.02.012
Received 2 November 2017; Received in revised form 22 February 2018; Accepted 25 February 2018
Available online 26 February 2018
2214-8604/

mechanism [15] do not require an excessive amount of a photopolymer, the vat still needs to be filled. The minimum amount of a photopolymer required to enable the process would be more significant if medical-grade materials are used or a newly synthesized material is used (which will typically have a very low yield ratio in particular in the initial stage of synthesis). Oxygen inhibition is a key issue in any type of polymerization processes, where a thin layer (1 μm–100 μm) of a material is cured in the ambient air, as the oxygen in the air near the material's surface can scavenge the radicals generated by a photoinitiator and prevent polymerization [18,19]. In general, a photopolymer with a low viscosity provides better reactive functionalities to interact between molecules, increased polymerization and crosslink reaction rates, and fast surface refreshing of a material, which reduces the fabrication time [20]. In contrast, a photopolymer with a higher viscosity requires a longer dwell and settling time, which lead to an increase in fabrication time. Therefore, the use of highly viscous photopolymers is a great huddle for vat-based MSL and, in general, a photopolymer with a low viscosity is recommended [10].

This work presents methods to overcome the aforementioned limitations. In particular, seeking a solution that utilizes as little photopolymers as possible, in an amount that is close to the volume of the largest microstructure which can be achieved within the building platform, was the main motivation of this work. In order to use smaller amounts of a photopolymer and overcome the disadvantages of vat-based MSL, a liquid bridge-based MSL (LBMSL) was proposed. A liquid bridge is a common natural phenomenon that can be easily created between two solid bodies [21,22]. When a liquid is introduced between two solid bodies, a stable bridge is formed which produces a resultant attractive force between the bodies (e.g. dewdrops between two leaves). This arises from a pressure deficiency in the bulk of the liquid and the surface tension of the liquid acting on the two bodies [23]. In this proposed method, no vat is used; instead, the liquid photopolymer is positioned between two parallel coaxial circular disks, forming a liquid bridge. In the LBMSL process, the amount of material consumption is significantly reduced, since no vat is used. Due to very short settling and dwelling times required, the fabrication speed has been dramatically improved. The following sections describe the methods and materials for realizing a liquid bridge, as well as the results for fabrication of various 3D microstructures in the proposed system.

2. Experimental program

2.1. Materials

Propoxylated glyceryl triacrylate (CD9021, with a viscosity of 95 cps at 25 °C), ethoxylated bisphenol A dimethacrylate (SR150, with a viscosity of 700 cps at 25 °C) and acrylated polyester oligomer (CN293, with a viscosity of 3200 cps at 25 °C) were obtained from Sartomer Inc. (Exton, PA, USA); 1,6-hexanediol diacrylate (HDDA) was obtained from Sigma-Aldrich Co. (Milwaukee, WI). These photopolymerizable chemicals were used as received without further purification. Tinuvin 327 (Ciba, Timonium, MD, USA) as a light absorber and 2,2-dimethoxy-2-phenylacetophenone (DMPA, Sigma-Aldrich Co.) as a photoinitiator were also used as received without further purification. For the adhesion test and liquid bridge validation, a mixture of CD9021 and HDDA in a 70:30 w/w ratio was used. For the viscosity testing, SR150 and CN293/HDDA in a 90:10 w/w ratio were used. Each photopolymer was prepared with a photopolymerizable chemical (or a mixture of the photopolymerizable chemicals) and DMPA (1 wt% to the mixture of photopolymerizable chemicals). For the fabrication of 3D microstructures, 0.15 wt% of Tinuvin 327 was blended into the photopolymer for cure depth control [2].

Plates composed of poly(methyl methacrylate) (PMMA), polydimethylsiloxane (PDMS), and TPX® (4-methylpentene-1-based olefin copolymer, Mitsui Chemicals, Inc.) were used as top and bottom substrates to form a liquid bridge. These plates were cut in a circular shape with a diameter of 8 mm.

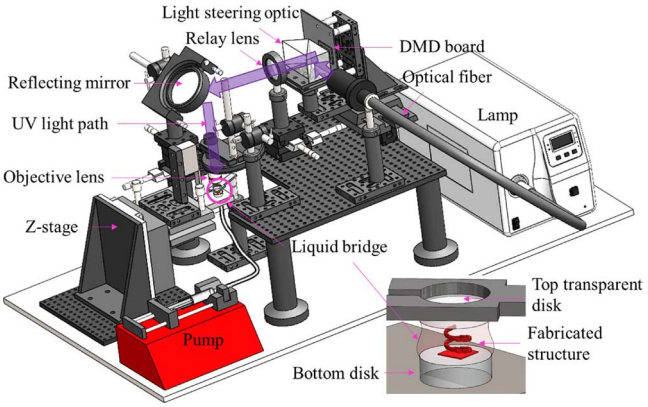

Fig. 1. Schematic illustration of the liquid bridge–based microstereolithography system.

2.2. Suggested liquid-bridge microstereolithography

LBMSL was implemented in the existing projection MSL system, where a digital micromirror device (DMD; Texas Instruments) was used for projection. [8] In brief, this system incorporates modules for light emission (a mercury lamp filtered at a wavelength of 365 nm, Omni-Cure® S2000, Excelitas Technologies Co.), light delivery (via a series of lenses and mirror), pattern generation (DMD and controller), and a build platform (a Z-stage with a resolution of 500 nm), as shown in Fig. 1. Details can be found in prior work [2,10,15,24,25]. A liquid bridge was formed between two parallel coaxial disks having the same diameter (8 mm) using a photopolymer that was supplied by a NE-1000 syringe pump (New Era Pump System Inc.) with a minimum pumping rate of 0.73 μL/hr. The top transparent disk was fixed, and the bottom disk was installed on a Z-stage. Fig. 2 shows a brief schematic of the LBMSL process, where the fabricated structure is attached to the bottom plate which moves downward after the completion of photocrosslinking in each layer.

2.3. Mathematical model of the liquid bridge

The liquid bridge can be modeled, and the profile of the bridge along the vertical direction can be calculated [26]. Fig. 3 shows the schematic diagram and the coordinate system used to model the liquid bridge [27]. This model was modified to further investigate how to form and maintain the bridge. The critical concern in the development of the suggested stacking mechanism is how to maintain the target area and thickness of a liquid bridge on a top surface that also provides a refreshed resin layer. This indicates how much material will need to be supplied as the height (h) between the disks increases. In addition, the maximum volume along with the maximum height are of interest, as this information provides a maximum build size for the manufacturing platform. A simulation can be conducted with the following Young–Laplace equations [27] to obtain the profile of the bridge, and the simulation results can be compared with the results obtained from the experiments for validation:

$$r''(s) = -z'(s)\beta'(s) \tag{1}$$

$$z''(s) = r'(s)\beta'(s) \tag{2}$$

$$\beta'(s) = -z(s) + \frac{\Delta P}{\sqrt{\rho g \gamma_p}} - \frac{z'(s)}{r(s)} \tag{3}$$

where, s is the arc length of the free surface, $r(s)$ is the radius of the bridge, $z(s)$ is the height from the substrate, $\beta(s)$ is the angle of the profile, ΔP is the Laplace pressure difference between the inside and outside of the liquid, ρ is the density of the liquid, g is the acceleration

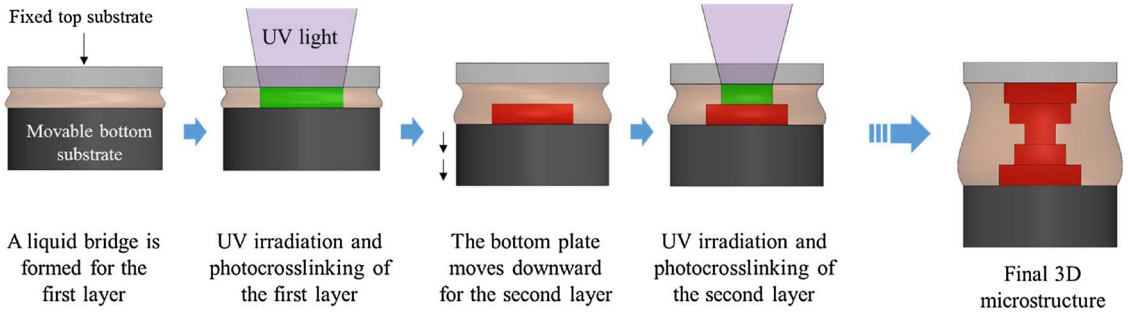

Fig. 2. Schematic illustration of the LBMSL process.

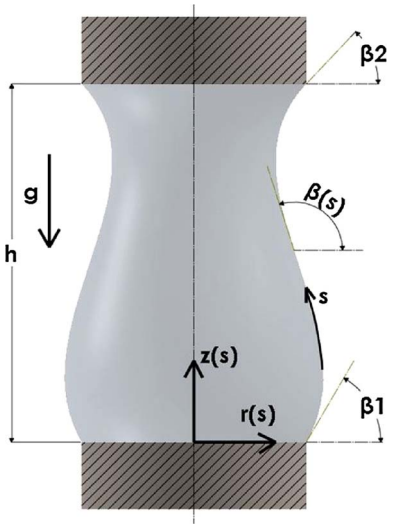

Fig. 3. Geometry and coordinate system for an axisymmetric equilibrium shape of a liquid bridge, where g is gravitational acceleration and $\beta 1$ and $\beta 2$ are the angles between the radius axis and the tangent of the liquid bridge interface.

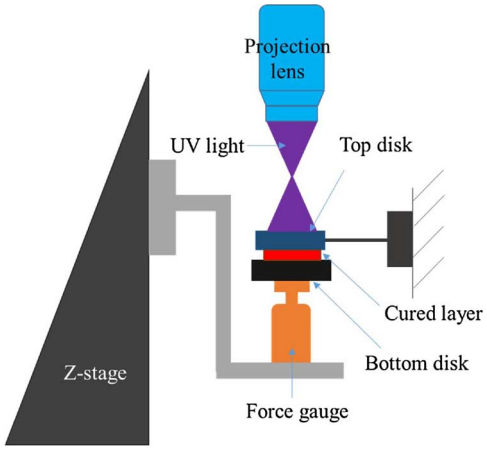

Fig. 4. Schematic illustration of setup for adhesion force test.

of gravity, γ_p is the surface tension of the photopolymer, and the prime is the differentiation with respect to the arc length (s).

To solve these equations, several boundary conditions such as $r(0) = r_0$, $r'(0) = cos\beta 1$, $z(0) = 0$, $z'(0) = sin\beta 1$ were used. These equations have been established with the assumption of the given constant volume ($\int_h^0 \pi r^2 dz = V$). And thus, a volume to be dispensed can be calculated by obtaining a new profile of the bridge with the modified parameters (such as h) while fixing the radius. MATLAB was adopted to integrate the equations. For a given r_0, the equilibrium shapes can be obtained for different disk separation h.

In order to validate the mathematical model, water was used to obtain the equilibrium shape and the volume for each $\beta 1$ of the liquid bridge. The parameters needed in this integration were as follows: $\rho = 1 \times 10^3$ kg/m^3, $\sigma = 0.072$ N/m, and $g = 9.8$ m/s^2. Different disk separation values h of 3 mm, 4 mm, and 5 mm were computed for the $\beta 1$ from 60° to 110° at intervals of 10°. The disks were cleaned by ethanol before conducting the experiment to minimize possible contamination and surfactant absorption, which may lead to Marangoni stresses [27,28]. The separation height (h) between the two disks was increased from 0 to 4 mm at intervals of 0.1 mm for the liquid bridge experiments.

2.4. Adhesion force between top disks and a fabricated layer

Bare glass, PDMS-coated glass, and TPX® were used as a top transparent disk for the adhesion tests. To enable the LBMSL process, the newly fabricated layer needs to successfully detach from the top disk without fracturing the structure, while the structure remains attached to the bottom disk. In the tests of this study, the top disks were fixed and the bottom disk (PMMA) was installed on a force gauge (GTX-250N, Dillon Force Measurement Equipment, Fairmont, MN, USA), which was mounted to the Z-stage, as shown in Fig. 4. The prepared photopolymer (CD9021/HDDA (70:30 w/w)) was injected from the bottom disk using a syringe pump. The separation distance between two disks was set to 100 μm. After the square pattern was solidified by ultraviolet (UV) curing, the stage moved down with a speed of 0.01 mm/s until the built structure separated from the top disk. Different exposure energies were used to cure the layer. Force data was collected at a sampling frequency of 20 Hz using a MATLAB program. Five data set were used for plotting.

2.5. Fabrication of 3D microstructures using LBMSL

The maximum size of the fabrication area was set at 3 mm × 3 mm, and the prepared photopolymer was supplied through a hole (material filling channel) machined in the bottom disk as shown in Fig. 5. The light irradiance was 9.6 mW/cm^2, and the exposure time was 2 s. Two photopolymers having different viscosities were used in the vat-based MSL and LBMSL systems. These tests were conducted in order to explore the fabrication capability of a highly viscous material. Finally, various 3D microstructures were built in the developed LBMSL system to show the demonstration of fabrication capabilities.

Bubbles can be created when the material is injected, which may create defects in the liquid bridge. To avoid this, the syringe was initially examined to remove all bubbles and the existing material in the tube was completely dispensed so that the new material coming from the syringe filled the tube. Sudden injection may create bubbles, and thus the lowest pumping rate (0.73 μL/hr) was used.

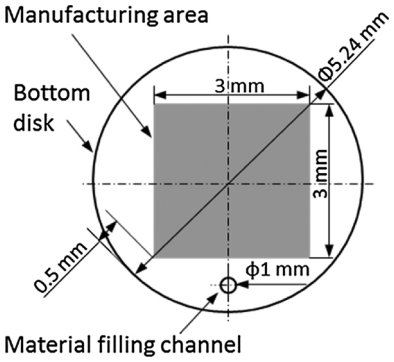

Fig. 5. Schematic illustration of a bottom disk for the LBMSL system. A gray square area is the maximum fabrication area for the system, and a hole of 1 mm diameter is the material injection channel.

3. Results and discussion

3.1. Liquid bridge model

Fig. 6 shows the equilibrium profiles of liquid bridges obtained from the simulations and experiments for different $\beta 1$ of water. The discrepancy between the mathematical model and the experimental results had an error percentage below 5%. From the comparison, the simulation results shows good agreement with the experimental results, which indicates that the mathematical model successfully predicts the equilibrium profile and the relationship between the height and the volume.

The validated model was used for the liquid bridge simulation for a mixture of CD9021 and HDDA (CD9021/HDDA). The volumes for various seperation distances (h) ranging from 0 to 3 mm to form a liquid bridge were obtained with $\beta 1$ of 70–120° using the mathematical model; the equilibrium shape and the volume with the height of 3 mm are presented in Fig. 7. These simulations provide a general guideline regarding how much material is supplied for a structure with a predetermined height and a given shape.

3.2. Adhesion test

The LBMSL technique is a top-down fabrication process. Ideally, after one layer is fabricated, the printed structure should safely separate from the top disk and move down with the bottom disk. However, the adhesion force produced during the polymerization process may result in separation failure. Three disks – bare glass, PDMS-coated glass, and TPX® – were used in this study in order to investigate the adhesion force between printed structures and top disks. Fig. 8 shows the comparisons of adhesion force for different top disks using different UV exposure times for a CD9021/HDDA (70:30 w/w) solution. The results indicate that the bare glass disk had a much higher adhesion force compared to PDMS-coated glass and TPX® disks, and the TPX® disk had the lowest adhesion force. This result is caused by the different free surface energy of the various disks; for a 3 s UV exposure time (Fig. 8(a)), the adhesion force of PDMS-coated glass and TPX® disks is similar, while the difference is greater for a 5 s UV exposure time (Fig. 8(b)). As the molecular weight of the polymer increases with UV exposure time, the adhesion properties of the polymer rise due to the increase in entanglements of the polymer molecules and the cohesive strength of the adhesive [29]. This result indicates that the TPX® disk is affected less by the adhesion properties as compared to bare glass and PDMS-coated glass disks, which results from the relatively small surface energy. Therefore, the TPX® disk is selected for the LBMSL process as a top disk due to its unique properties such as low surface energy, high chemical resistance, and high UV transmittance.

3.3. Oxygen inhibition

In the vat-based MSL process, a thin layer of a photopolymer (1–20 μm) is cured in the ambient air; thus, a very thin layer (≤1 μm) of photopolymers is directly affected by oxygen inhibition during its polymerization process [18,19]. However, LBMSL allows a very thin layer (≤1 μm) to be fabricated, as a top disk is able to prevent the top surface of the resins from coming into direct contact with oxygen. By using LBMSL, vertical posts were fabricated with CD9021/HDDA (70:30 w/w), as shown in Fig. 9. The posts consist of four sections along the vertical direction with varying layer thicknesses (0.5, 1, 10, and 20 μm) for each section from top to bottom. The height of each section was set to 200 μm. For the sections having layer thicknesses of 0.5 and 1 μm, a very smooth (almost layerless) surface was achieved, while sections having larger layer thicknesses exhibit clear layering.

3.4. Use of highly viscous photopolymers

Photopolymers with different viscosities were used in order to compare the manufacturability between vat-based MSL and LBMSL. Fig. 10 shows spring structures fabricated using SR150 and a mixture of CN293/HDDA (90:10 w/w). The viscosity of those solutions at 25 °C is 700 and 3200 cP, respectively. For the spring structure of SR150 fabricated by vat-based MSL (Fig. 10(a)), the layer thickness is 20 μm and the number of layers is 175. After one layer of fabrication, the platform is moved down for 2 mm and stays for a dwell time of 5 s and then moved up for 1.98 mm with a settling time of 30 s, which was empirically chosen. This process is generally called “deep-dip coating.” The time for fabricating each layer was 77 s; fabrication time for a structure with 175 layers was 3.74 h, including the time required for stage movement, exposure time, dwell time, and settling time. The spring structure in Fig. 10(b) was fabricated by the LBMSL system using SR150. After one layer was fabricated, the bottom disk was lowered 0.4 mm at a speed of 0.1 mm/s in order to force the built layer to separate completely from the top disk; the bottom disk was then raised 0.38 mm with a settling time of 8 s to allow the liquid bridge to stabilize before the next layer was fabricated. The time required for fabricating each layer was 20 s, and the entire fabrication time was 0.87 h, which is 3.8 times faster than the time required for vat-based MSL.

In addition to SR150, a higher viscosity material, CN293/HDDA (90:10 w/w) was used to fabricate the same structure using both systems. For vat-based MSL, the dwell and settling times were set to 10 s and 60 s, respectively, and the fabrication time for each layer was 112 s (for a total fabrication time of 5.4 h). The diameter of the spring wire in Fig. 10(c) was approximately 700 μm, which is larger than the 500 μm diameter of the designed model. This difference is attributed to insufficient settling time, leading to an uneven polymer surface, which may make the curing spot above the focus level. Since the light pattern from the objective lens was convergent, the curing spot above the focus level could result in a larger curing area than is achieved on the focus level. A distorted scale and uneven surface features were observed, which resulted from insufficient dwell and settling times. For LBMSL, the settling time was 12 s, and the other parameters were the same as those used in vat-based MSL. The fabrication time for each layer was 22 s, and the total fabrication time was 1.07 h, which is 5 times less than the time required for vat-based MSL. Compared with the spring fabricated using vat-based MSL, the spring fabricated using LBMSL had much better features in terms of resolution. Stair structures are clearly visible on the spring surface, as shown in Fig. 10(d).

The settling time increases significantly when a more highly viscous material is used in vat-based MSL, while less time is required for settling of the photopolymer in LBMSL. Therefore, LBMSL exhibits a huge potential for fabrication with a highly viscous material, which can significantly broaden the range of materials that can be processed as compared to those for a vat-based MSL process.

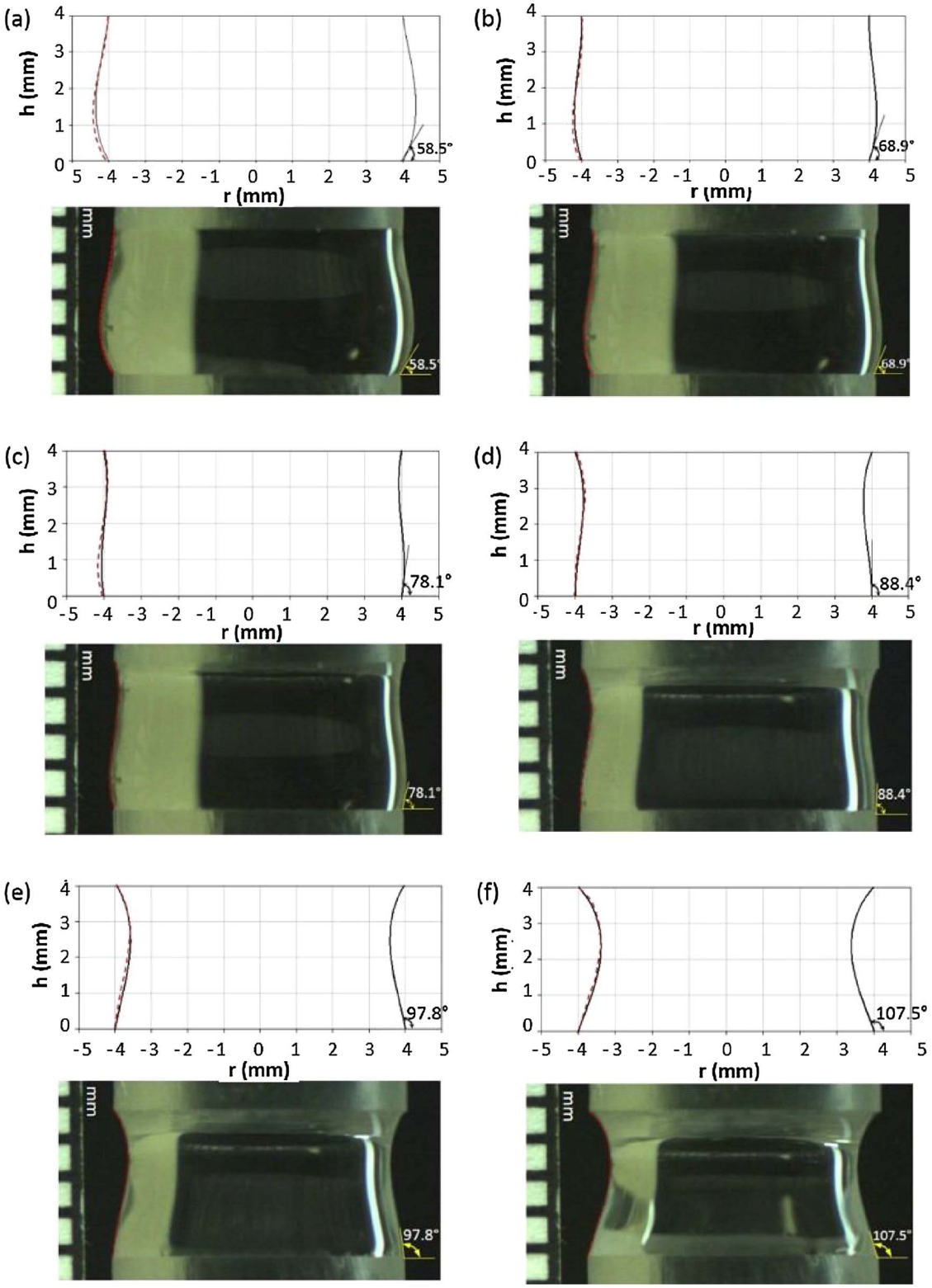

Fig. 6. Equilibrium shapes of liquid bridges for water obtained from simulations and experiments with various $\beta 1$; (a) 58.5°, (b) 68.5°, (c) 78.1°, (d) 88.4°, (e) 97.8°, and (f) 107.5°. (The red dashed lines on the plots indicate the outer shape of each liquid bridge as obtained from the experiments. They were mapped in the simulation results.). (For interpretation of the references to colour in this figure legend, the reader is referred to the web version of this article.)

3.5. Fabricated 3D microstructures

Before the fabrication of 3D microstructures for the demonstration of the LBMSL capabilities, the system was manually calibrated. Due to the top transparent plate, there is a possibility for light scattering which may make changes in the focal plane and resolution of the focused light. The exact focal plane was obtained by having experiments on patterning 2D shapes with different vertical locations of the substrate. In addition, resolutions of 2D patterns were compared with those from the original MSL and it was concluded that there was no remarkable

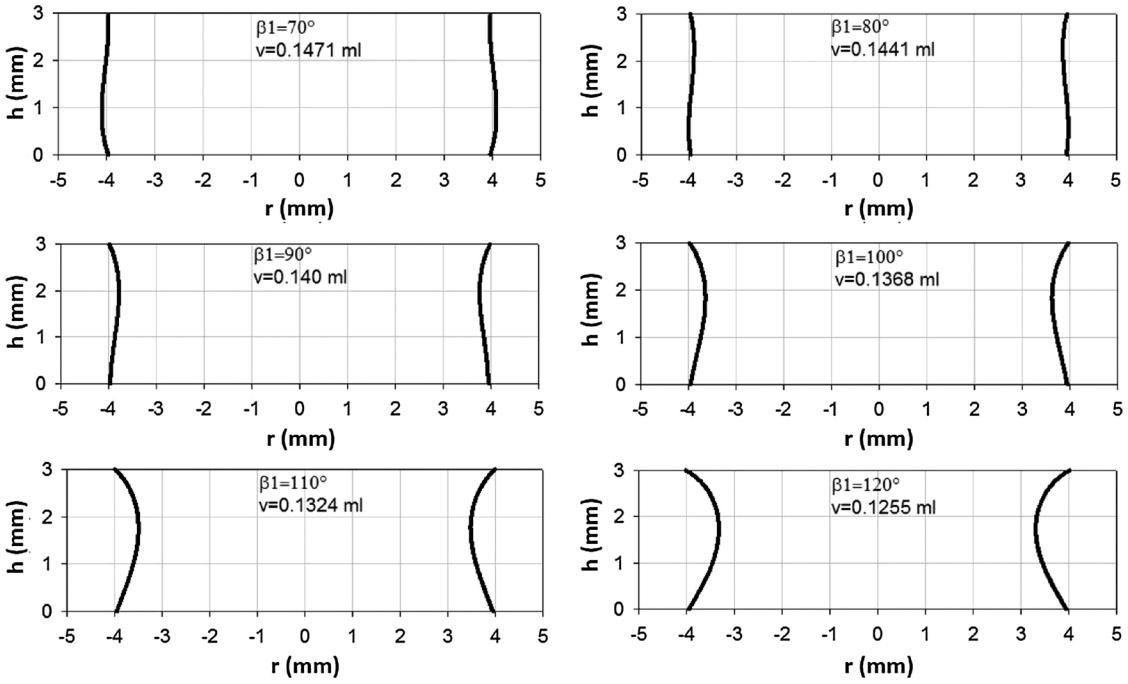

Fig. 7. The equilibrium shape and coresponding volume of CD9021/HDDA liquid bridges obtained using a mathematical model.

difference in the resolution.

Fig. 11 shows environmental scanning electron microscopy (ESEM) images of multiple 3D microstructures fabricated using LBMSL and a mixture of CN293/HDDA. The printing parameters were chosen to be compatible with the photopolymer used, which were taken from our prior work [2,10,15,24,25]. A layer thickness of 10 μm was used in all the models. An exposure energy of ~9.3 mJ/cm^2 (intensity of ~ 18.6 mW/cm^2, and exposure time of 0.5 s) was used to cure each layer. The Z-stage was moved downward with the speed of 0.5 m/s and the distance of 1 mm in each layer for detachment and then moved upward, leaving the layer thickness. The numbers of layers in the parts (a)–(d) are 120, 110, 138, and 155, respectively. The thinnest feature sizes in the parts (a)–(d) are ~60 μm, 100 μm, 140 μm, and 200 μm, respectively. The volume of the photopolymer to create a liquid bridge was ~0.25 mL. After the printing process was complete, each structure was rinsed with ethanol to wash away any remaining uncured resins. All fabricated microstructures showed detailed features, which demonstrate the superior manufacturing capability.

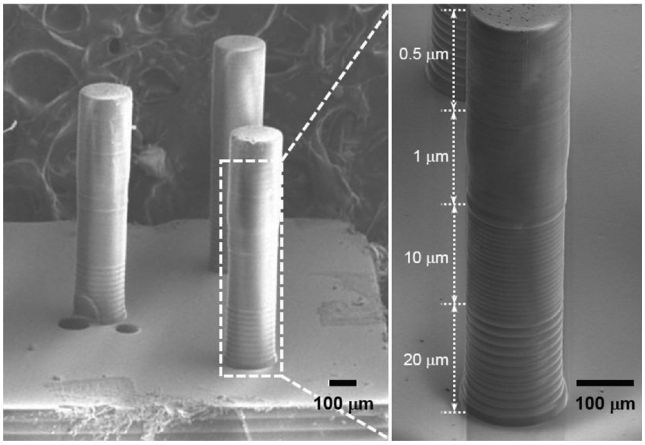

Fig. 9. 3D printed CD9021/HDDA posts (70:30 w/w) consisting of four sections with layer thicknesses ranging from 0.5 to 20 μm.

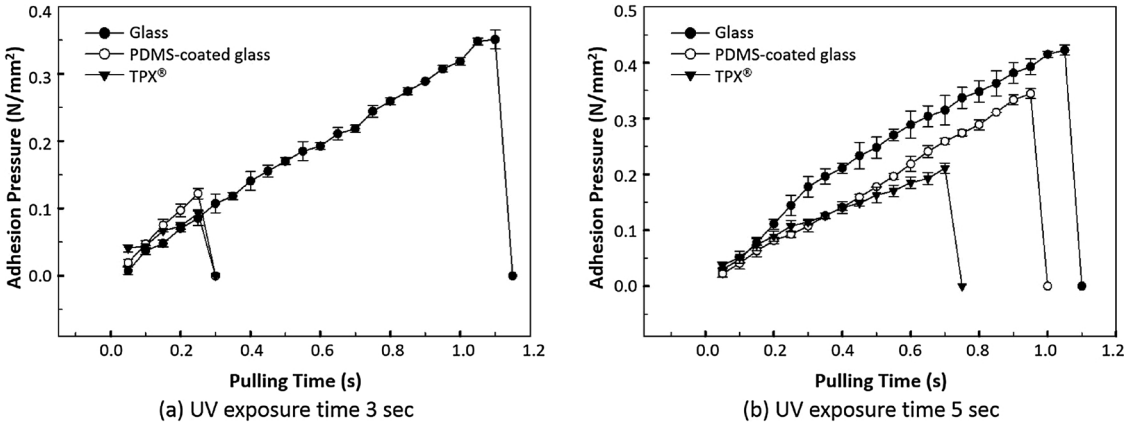

Fig. 8. Adhesion force between printed structures (UV cured during (a) 3 s and (b) 5 s) and different top disks (glass, PDMS-coated glass, and TPX®) at a pulling speed of 0.01 mm/s.

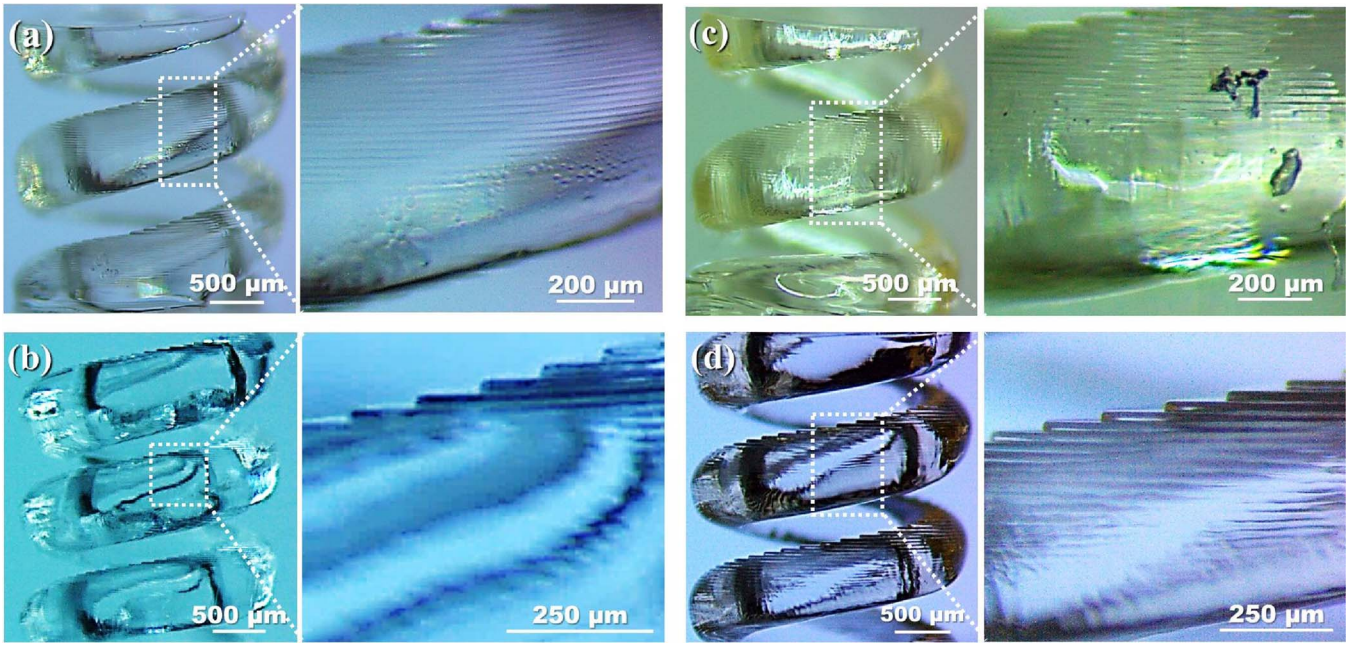

Fig. 10. Spring structures fabricated from SR150 by using (a) vat-based MSL and (b) LBMSL; spring structures fabricated from CN293/HDDA (90:10 w/w) by using (c) vat-based MSL and (d) LBMSL.

4. Conclusions

The novel LBMSL process showed advantages in terms of the fabrication speed, capability for fabrication using materials of high viscosity and in submicron layer thicknesses, with lower material consumption. This advanced process improved the fabrication capacity of MSL and demonstrated that it could be used for a wider range of applications. The liquid bridge was mathematically modeled, and the profile of the bridge was simulated. A series of experiments to verify the mathematical model were conducted, and the predictions of the

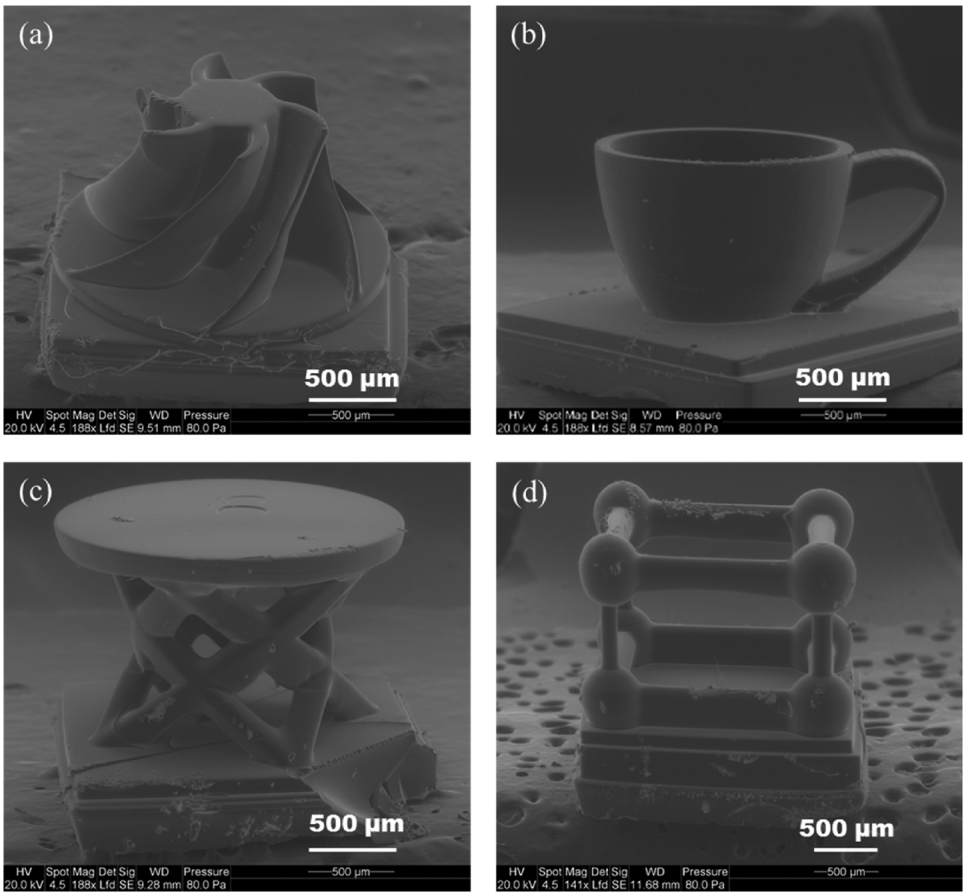

Fig. 11. Scanning electron micrographs of the fabricated 3D microstructures.

developed model showed good agreement with the experimental results. Using the developed process, several microstructures were fabricated to demonstrate the fabrication capacity of LBMSL. It is believed that the developed process could be considered as a potential 3D microfabrication method with high resolution using materials with high viscosity, which cannot be easily employed in conventional MSL processes.

Acknowledgements

This work was supported by a grant from Faculty Research Committee of The University of Akron and was partially supported by the National Science Foundation under grant no. CMMI MME-1636118. It is noted that Jeongwoo Lee and Yanfeng Lu have an equal contribution as a co-first author.

References

[1] K. Ikuta, K. Hirowatari, Ieee, Real 3-dimensional microfabrication using stereo lithography and metal molding. Micro electro mechanical systems, Proceedings: an Investigation of Micro Structures, Sensors, Actuators, Machines, and Systems (1993) 42–47.
[2] J.W. Choi, R.B. Wicker, S.H. Cho, C.S. Ha, S.H. Lee, Cure depth control for complex 3D microstructure fabrication in dynamic mask projection microstereolithography, Rapid Prototyp. J. 15 (1) (2009) 59–70.
[3] A. Bertsch, H. Lorenz, P. Renaud, 3D microfabrication by combining microstereolithography and thick resist UV lithography, Sens. Actuators A-Phys. 73 (1–2) (1999) 14–23.
[4] S. Deshmukh, P.S. Gandhi, Optomechanical scanning systems for microstereolithography (MSL): Analysis and experimental verification, J. Mater. Process. Technol. 209 (3) (2009) 1275–1285.
[5] P.S. Gandhi, S. Deshmukh, A 2D optomechanical focused laser spot scanner: analysis and experimental results for microstereolithography, J. Micromech. Microeng. 20 (1) (2010).
[6] X. Zhang, X.N. Jiang, C. Sun, Micro-stereolithography of polymeric and ceramic microstructures, Sens. Actuators A-Phys. 77 (2) (1999) 149–156.
[7] C.J. Pateman, A.J. Harding, A. Glen, C.S. Taylor, C.R. Christmas, P.P. Robinson, S. Rimmer, F.M. Boissonade, F. Claeyssens, J.W. Haycock, Nerve guides manufactured from photocurable polymers to aid peripheral nerve repair, Biomaterials 49 (2015) 77–89.
[8] Y. Lu, S.N. Mantha, D.C. Crowder, S. Chinchilla, K.N. Shah, Y.H. Yun, R.B. Wicker, J.W. Choi, Microstereolithography and characterization of poly(propylene fumarate)-based drug-loaded microneedle arrays, Biofabrication 7 (4) (2015).
[9] M.S. Evangelista, M. Perez, A.A. Salibian, J.M. Hassan, S. Darcy, K.Z. Paydar, R.B. Wicker, K. Arcaute, B.K. Mann, G.R.D. Evans, Single-lumen and multi-lumen poly(ethylene glycol) nerve conduits fabricated by stereolithography for peripheral nerve regeneration In vivo, J. Reconstr. Microsurg. 31 (5) (2015) 327–335.
[10] J.W. Choi, R. Wicker, S.H. Lee, K.H. Choi, C.S. Ha, I. Chung, Fabrication of 3D biocompatible/biodegradable micro-scaffolds using dynamic mask projection microstereolithography, J. Mater. Process. Technol. 209 (15–16) (2009) 5494–5503.
[11] I.A. Barker, M.P. Ablett, H.T.J. Gilbert, S.J. Leigh, J.A. Covington, J.A. Hoyland, S.M. Richardson, A.P. Dove, A microstereolithography resin based on thiol-ene chemistry: towards biocompatible 3D extracellular constructs for tissue engineering, Biomater. Sci. 2 (4) (2014) 472–475.
[12] J.A.S. Neiman, R. Raman, V. Chan, M.G. Rhoads, M.S.B. Raredon, J.J. Velazquez, R.L. Dyer, R. Bashir, P.T. Hammond, L.G. Griffith, Photopatterning of hydrogel scaffolds coupled to filter materials using stereolithography for perfused 3D culture of hepatocytes, Biotechnol. Bioeng. 112 (4) (2015) 777–787.
[13] L.W. Liu, W.Y. Ieee, Fabrication of three dimensional hollow or suspended microstructures, 2014 International Symposium on Micro-Nanomechatronics and Human Science (Mhs) (2014).
[14] A.K. Au, W. Lee, A. Folch, Mail-order microfluidics: evaluation of stereolithography for the production of microfluidic devices, Lab Chip 14 (7) (2014) 1294–1301.
[15] J.W. Choi, E. MacDonald, R. Wicker, Multi-material microstereolithography, Int. J. Adv. Manuf. Technol. 49 (5–8) (2010) 543–551.
[16] J.W. Choi, H.C. Kim, R. Wicker, Multi-material stereolithography, J. Mater. Process. Technol. 211 (3) (2011) 318–328.
[17] Z. Chi, C. Yong, Y. Zhigang, K. Behrokh, Digital material fabrication using mask-image-projection-based stereolithography, Rapid Prototyp. J. 19 (3) (2013) 153–165.
[18] S.C. Ligon, B. Husar, H. Wutzel, R. Holman, R. Liska, Strategies to reduce oxygen inhibition in photoinduced polymerization, Chem. Rev. 114 (1) (2014) 557–589.
[19] M.A. Gauthier, I. Stangel, T.H. Ellis, X.X. Zhu, Oxygen inhibition in dental resins, J. Dent. Res. 84 (8) (2005) 725–729.
[20] R.J. Mondschein, A. Kanitkar, C.B. Williams, S.S. Verbridge, T.E. Long, Polymer structure-property requirements for stereolithographic 3D printing of soft tissue engineering scaffolds, Biomaterials 140 (Suppl. C) (2017) 170–188.
[21] L.A. Slobozhanin, J.M. Perales, Stability of liquid bridges between equal disks in an axial gravity-field, Phys. Fluids A-Fluid Dyn. 5 (6) (1993) 1305–1314.
[22] A. Sanz, I. Martinez, Minimum volume for a liquid bridge between equal disks, J. Colloid Interface Sci. 93 (1) (1983) 235–240.
[23] G.P. Lian, C. Thornton, M.J. Adams, A theoretical-study of the liquid bridge forces between 2 rigid spherical bodies, J. Colloid Interface Sci. 161 (1) (1993) 138–147.
[24] J.W. Choi, M. Yamashita, J. Sakakibara, Y. Kaji, T. Oshika, R.B. Wicker, Combined micro and macro additive manufacturing of a swirling flow coaxial phacoemulsifier sleeve with internal micro-vanes, Biomed. Microdevices 12 (5) (2010) 875–886.
[25] J.W. Choi, M.D. Irwin, R.B. Wicker, In DMD-based 3D Micro-manufacturing, Conference on Emerging Digital Micromirror Device Based Systems and Applications II, San Francisco, CA, Jan 27; San Francisco, CA, 2010.
[26] H. Chen, A. Amirfazli, T. Tang, Modeling liquid bridge between surfaces with contact angle hysteresis, Langmuir 29 (10) (2013) 3310–3319.
[27] B.A. Qian, K.S. Breuer, The motion, stability and breakup of a stretching liquid bridge with a receding contact line, J. Fluid Mech. 666 (2011) 554–572.
[28] W.R. Hu, J.Z. Shu, R. Zhou, Z.M. Tang, Influence of liquid bridge volume on the onset of oscillation in floating-zone convection .1. Experiments, J. Cryst. Growth 142 (3–4) (1994) 379–384.
[29] J. Kajtna, J. Golob, M. Krajnc, The effect of polymer molecular weight and cross-linking reactions on the adhesion properties of microsphere water-based acrylic pressure-sensitive adhesives, Int. J. Adhes. Adhes. 29 (2) (2009) 186–194.